Published in final edited form as:
Science. 2010 January 15; 327(5963): 331–334. doi:10.1126/science.1179907.

Tetrathiomolybdate Inhibits Copper Trafficking Proteins Through Metal Cluster Formation

Hamsell M. Alvarez[1,*], **Yi Xue**[1,*], **Chandler D. Robinson**[1], **Mónica A. Canalizo-Hernández**[1], **Rebecca G. Marvin**[1], **Rebekah A. Kelly**[3], **Alfonso Mondragón**[2], **James E. Penner-Hahn**[3], and **Thomas V. O'Halloran**[1,2,†]

[1]The Chemistry of Life Processes Institute, Northwestern University, Evanston, IL 60208, USA

[2]Department of Biochemistry, Molecular Biology and Cell Biology, Northwestern University, Evanston, IL 60208, USA

[3]Department of Chemistry, The University of Michigan, Ann Arbor, MI 48109, USA

Abstract

Tetrathiomolybdate (TM) is an orally active agent for treatment of disorders of copper metabolism. Here we describe how TM inhibits proteins that regulate copper physiology. Crystallographic results reveal that the surprising stability of the drug complex with the metallochaperone Atx1 arises from formation of a sulfur-bridged copper-molybdenum cluster reminiscent of those found in molybdenum and iron sulfur proteins. Spectroscopic studies indicate that this cluster is stable in solution and corresponds to physiological clusters isolated from TM-treated Wilson's disease animal models. Finally, mechanistic studies show that the drug-metallochaperone inhibits metal transfer functions between copper-trafficking proteins. The results are consistent with a model wherein TM can directly and reversibly down-regulate copper delivery to secreted metalloenzymes and suggest that proteins involved in metal regulation might be fruitful drug targets.

Excess dietary molybdate (MoO_4^{2-}) uptake was first linked to a fatal disorder in cattle known as "teart" pastures syndrome (1) and later to a neurological disorder in sheep known as "swayback" (2). Both disorders arise from Mo-induced copper deficiency, and the symptoms are readily reversed with copper supplementation. Although molybdate itself has little or no affinity for copper ions, the active copper-depleting agent, TM (MoS_4^{2-}), is formed in the ruminants' digestive track and readily reacts with Cu^{I} or Cu^{II} to form insoluble compounds. These zoogenic studies inspired the development of molybdenum compounds to treat copper-dependent diseases in humans (3). The potent chelating and antiangiogenic activities of orally active formulations of TM, such as the ammonium salt [$(NH_4)_2(MoS_4)$] (4–6) and the choline salt (ATN-224) (7, 8), have been used in treatment of Wilson's disease, where copper accumulation leads to hepatic and neurological disorders, as well as in the inhibition of metastatic cancer progression in a number of clinical trials (9–11). TM inhibits several copper enzymes, including ceruloplasmin (Cp), ascorbate oxidase,

†To whom correspondence should be addressed: t-ohalloran@northwestern.edu.
*These authors contributed equally to this work.

Supporting Online Material
www.sciencemag.org/cgi/content/full/science.1179907/DC1
Materials and Methods
Fig. S1 to S16
Table S1 to S4
References
Movie S1

cytochrome oxidase, superoxide dismutase (SOD1), tyrosinase, and the *Enterococcus hirae* adenosine triphosphatase (ATPase) (CopB) (12, 13), and also down-regulates the expression of cytokines, such as the vascular endothelial growth factor, as well as transcription factors, such as nuclear factor κB, involved in angiogenesis signaling pathways (14, 15). Although TM can bind to Cu-Cp (12), copper–bovine serum albumin (Cu-BSA) (16), and Cu-containing metallothioneins (Cu-MT) (17) and has been proposed to inhibit SOD1 by partially removing copper from the enzyme (8, 18), the reaction chemistry and structures of these complexes have not been resolved.

Metallochaperones constitute a particular kind of protein that delivers metal ions to specific cytoplasmatic targets in the cell (19). The prototypical metallochaperone, yeast Atx1, transfers Cu^I along a trafficking pathway via electrostatic interactions with structurally homologous N-terminal domains of the ATPase, Ccc2 (20, 21). Likewise, the closely related human copper metallochaperone, antioxidant 1 (Atox1), can transfer copper to N-terminal domains of the copper-transporting ATPases 7a and 7b, also known as the Menkes and Wilson disease proteins. All three of these proteins are important in mammalian copper homeostasis and provide copper to secreted enzymes that are important in vascular integrity such as Cp and extracellular SOD (ecSOD). We anticipated that TM would readily remove Cu^I from its binding site in Atx1 with subsequent formation of a typical polymeric CuMo sulfide precipitate. We found instead a robust TM-metallochaperone complex with metal sulfur ratios reminiscent of the FeMo cofactor complex in nitrogenase (22) and elucidated how this anti-angiogenic drug affects the structure and function of a canonical metal-trafficking domain.

Direct reaction of TM with Cu-Atx1 leads to rapid formation of an air-stable purple complex that can be readily isolated by size-exclusion chromatography (23). Crystals of this complex diffract to 2.3 Å (fig. S1), and the x-ray structure reveals the presence of 12 Cu-Atx1 molecules in the asymmetric unit arranged as four TM-Cu-Atx1 noncrystallographic trimers (fig. S2). The overall structure of each Atx1 monomer is similar to previously determined structures, retaining the "ferredoxin-like" βαββαβ fold (24), with two cysteines involved in copper binding (Cys^{15} and Cys^{18}) located at the protein surface. Superposition of the coordinates of Hg-Atx1 (PDB code 1CC8) (24) and Cu-Atox1 (human analog of Atx1, PDB code 1FEE) (25) on the monomers in the complex (Fig. 1, C and D) reveals that the peptide fold around the metal-binding loop is unperturbed by TM binding, with an average root mean square deviation for the C_α atoms of ~0.67 Å (Hg-Atx1) and ~1.3 Å (Cu-Atox1). In the structure, each Atx1 trimer coordinates four copper atoms and one TM molecule, with the stoichiometry $[TM][(Cu)(Cu\text{-}Atx1)_3]$, which is corroborated by independent elemental analysis of the complex (23). The Cu x-ray absorption near-edge structure of the complex indicates that the copper remains in the Cu^I oxidation state, whereas the Mo K near-edge spectrum strongly resembles that of tetrathiomolybdate (Mo^{VI}) (fig. S3). Aside from a few H-bonding interactions between monomers, the dominant forces stabilizing the trimer are the coordinate covalent bonds between the protein CysS atoms and the metal cluster.

A "nest-shaped" copper-molybdenum cluster, unprecedented in metalloproteins, is located at the center of the Atx1 trimer (Fig. 1, A and B) on the threefold axis. The cluster consists of four Cu^I ions, $[MoS_4]^{2-}$, and three pairs of Atx1 CysS atoms to give a $[S_6Cu_4MoS_4]$ cluster (Fig. 2). The Mo atom remains tetrahedrally coordinated by four sulfide ions with Mo–S distances in the range 2.18 to 2.26 Å (mean: 2.22 Å), as expected for Cu–S–Mo cluster interactions and commensurate with the ones observed in the parent drug (2.17 to 2.20 Å, mean: 2.19 Å) (7). Three of the copper atoms bind to the sulfur atoms of cysteines 15 and 18, and each of these atoms also binds two sulfides from $[MoS_4]^{2-}$, which results in a distorted tetrahedral coordination environment for the coppers with similar distances for the Cu-S bonds to protein side chains (2.21 to 2.44 Å, mean: 2.30 Å) or the sulfides of TM (2.24

to 2.40 Å, mean: 2.29 Å). The Mo-Cu distances are in the range of 2.74 to 2.82 Å (mean: 2.77 Å). The fourth sulfide of TM does not coordinate copper or interact with protein. On the other side of the complex, the fourth copper atom is bound by three (Cys^{15})S_γ atoms (2.22 to 2.30 Å, mean: 2.26 Å) and exhibits a trigonal planar coordination. Thus, three of the four sulfide ions in TM form a μ_3-S bridge between the Mo atom and two tetrahedral Cu atoms, whereas each of the (Cys^{15})S_γ atoms of three Atx1 behave as a bridging ligand between one tetrahedral and one trigonal planar copper center. In the tetrahedrally coordinated coppers, the (Cys^{15})S_γ–Cu–S_γ(Cys18) bond angles are larger (118° to 125°, mean: 122°) than the (TM)S–Cu–S(TM) bond angles (99° to 103°, mean: 101°), consistent with a distorted tetrahedral site. The geometry at the Mo atom is only slightly distorted from tetrahedral, with (TM)(μ_3-S)–Mo–(μ_3-S)(TM) and (TM)(μ_3-S)–Mo–S(TM) bond angles of 103° to 110° (mean: 106°) and 109° to 116° (mean: 112°), respectively. Protein-TM interactions partially neutralize the negative charge delocalized over the $[Cu_4MoS_4]^{4-}$ cluster (fig. S4 and Fig. 2A). Three positively charged lysines (Lys^{65}), one from each Atx1 monomer, form hydrogen bonds with the sulfides from TM and the thiolates of Cys^{18}. Strong interactions are observed for the only terminal S thiolate ligand in the cluster (Cys^{18}–S–Lys^{65}–Nζ = 3.3 Å) relative to μ_3-S bridging sulfide ligands (TM–μ_3-S–Lys^{65}–Nζ = 3.8 Å). In addition, H bonds from backbone amides (Thr^{14} and Gly^{17}) at the amino terminus of α helix 2 to metal-bound thiolates further neutralize the negative charge of the buried cluster.

Although this type of cluster has not been previously reported in metalloproteins, analogous nest-shaped $[Cu_3MoS_3O]$ inorganic units (with P- and N-donor ligands) are components of larger clusters (26). The closest fragment analog of the protein-drug adduct is a component of the $[Bu^n{}_4N]_4[Cu_{12}Mo_8S_{32}]$ complex. Here, a $[S_6Cu_3MoS_4]$ unit exhibits similar cluster framework with Mo–Cu distances from 2.69 to 2.75 Å, Mo–S distances from 2.06 to 2.25 Å and Cu–S distances from 2.29 to 2.36 Å (27) (fig. S5). Another structurally distinct CuSMo center is observed in the Cu-Mo-pterin enzyme carbon monoxide dehydrogenase from *Oligotropha carboxidovorans*, where a single diagonally coordinated Cu atom is bound via a bridging sulfide to a Mo active site forming a [CuSMo(=O)OH] cluster (28).

To determine whether TM interaction with Atx1 inhibits its copper chaperone activity, we developed a native gel–based copper transfer assay that monitors metal occupancy in a mixture of TM-Cu-Atx1 trimer and Ccc2a, the physiological partner of Atx1 (fig. S6). The assay takes advantage of the fact that apo- and Cu-Atx1 are clearly distinguishable from Ccc2a and TM-Cu-Atx1 in a native agarose gel system (23), where the protein and metal content of the bands are characterized by a variety of analytical techniques to establish the metallation state of each protein (fig. S7 to S12 and table S1). The assay was validated by a combination of electrospray ionization protein mass spectrometry (ESI-MS) and quantitative elemental analysis via inductively coupled plasma MS (ICP-MS) of samples extracted from gel slices, as well as by qualitative laser scanning elemental analysis, that is, laser ablation with ICP-MS (LA-ICP-MS) of the electrophoresis gel itself. Three key lanes are shown in Fig. 3A. The TM-Cu-Atx1(SeMet) migrates as a positive species containing copper and molybdenum (lane I). Mixing of apo-Ccc2a and Cu-Atx1 (SeMet) results in the transfer of copper from Cu-Atx1(SeMet) to Ccc2a (lane II). The transfer of copper from Atx1(SeMet) to Ccc2a is almost completely abolished by the presence of TM (lane III). Both native Atx1 and the SeMet analog give similar results. It is intriguing that protein analysis indicates formation of a new Cu-TM protein complex that contains the Ccc2 domain, as well as TM and Cu-Atx1. The formation of this heteromeric protein complex suggests that other proteins with a surface-exposed MxCxxC copper-binding motif will be able to form similar complexes with TM.

These results suggest a new model for how a drug can disrupt a key protein-protein interaction for metal-trafficking pathways. Support for the physiological occurrence of this type of metal-protein cluster is shown in Fig. 3B by the highly similar Cu and Mo K-edge extended x-ray absorption fine structure analysis of the [TM][(Cu)(Cu-Atx1)$_3$] complex, and a kidney sample extracted from TM-treated LPP rats (animal model of Wilson's disease), where a similar [(CuSR)$_3$S$_4$Mo]$^{2-}$-type interaction is proposed (29). The stoichiometry of three chaperone molecules and four copper atoms per drug molecule has several physiological implications. By sequestering multiple copper chaperones and the metal cargo destined for trafficking to the trans-Golgi, TM may suppress Cu incorporation into secreted copper enzymes, including those involved in modification of the vasculature such as ecSOD, copper amine oxidases, lysyl oxidase, and Cp. The TM-mediated sequestration of copper-loaded metallochaperones may perturb other proposed roles of Atox1 in regulation of copper-related tumor angiogenic factors (30).

The structure and biochemistry of the TM-Cu-Atx1 complex also provides chemical insights into the puzzling stoichiometry of the dietary Cu-Mo antagonism (31) and suggests why ternary complex formation between TM and specific Cu proteins can have pronounced physiological consequences (32). A relatively small amount of dietary molybdenum clearly perturbs the timely dissemination of a larger pool of copper in deficiency disorders such as swayback and teart pasture syndrome. Our results raise the possibility that the active agent, TM, functionally suppresses copper trafficking domains that control the secretion of the active forms of copper-dependent enzymes. Finally, our results suggest that proteins involved in such metallation pathways may be targets for the development of new classes of pharmaceutical agents.

Supplementary Material

Refer to Web version on PubMed Central for supplementary material.

Acknowledgments

This manuscript is dedicated to the memory of E. Stiefel and his contributions to the field of molybdenum sulfide chemistry. This work was supported by grant GM54222 and GM38784 (T.V.O.) and GM38047 (J.E.P.-H.) from the NIH. The Robert H. Lurie Comprehensive Cancer Center provided a Malkin Fellowship (H.M.A.) and support for Structural Biology Facility. Use of the Advanced Photon Source [Structural Biology Center-Collaborative Access Team (CAT) and Industrial Macromolecular Crystallography Association CAT] and the Stanford Synchrotron Radiation Laboratory (SSRL) was supported by the U.S. Department of Energy, Office of Basic Energy Sciences, with additional support (at SSRL) from the National Center for Research Resources, NIH. Use of the Chicago Biomedical Consortium (CBC)–University of Illinois at Chicago Proteomics Facility was supported by The Searle Funds at the CBC, and use of LA-ICP-MS was supported by a National Aeronautics and Space Administration grant to the Quantitative Bioelement Imaging Center in the Chemistry of Life Processes Institute at Northwestern University. We thank P. Focia for assistance with x-ray diffraction collection, M. Clausén for assistance in the early stages of XAS measurements, Y. Wang for assistance with the protein MS, A. Davis for providing *apo*-Ccc2a, and A. Mazar for helpful discussions. The atomic coordinates have been deposited at the Protein Data Bank with code 3K7R.

References and Notes

1. Ferguson WS, Lewis AH, Watson SJ. Nature. 1938; 141:553.
2. Mills CF, Fell BF. Nature. 1960; 185:20. [PubMed: 14422643]
3. Brewer GJ. Exp Biol Med (Maywood). 2001; 226:665. [PubMed: 11444102]
4. Walshe, JM. Orphan Diseases and Orphan Drugs. Scheinberg, IH.; Walshe, JM., editors. Manchester Univ. Press; Manchester, UK: 1986. p. 76-85.
5. Brewer GJ, et al. Arch Neurol. 1991; 48:42. [PubMed: 1986725]

6. Sadler, PJ.; Muncie, C.; Shipman, MA. Biological Inorganic Chemistry: Structure and Reactivity. Bertini, I.; Gray, HB.; Stiefel, EI.; Valentine, JS., editors. University Science Books; Sausalito, CA: 2007. p. 95-135.
7. Lee VE, Schulman JM, Stiefel EI, Lee CC. J Inorg Biochem. 2007; 101:1707. [PubMed: 17804073]
8. Juarez JC, et al. Clin Cancer Res. 2006; 12:4974. [PubMed: 16914587]
9. Brewer GJ, et al. Clin Cancer Res. 2000; 6:1. [PubMed: 10656425]
10. Redman BG, et al. Clin Cancer Res. 2003; 9:1666. [PubMed: 12738719]
11. Active trials: TM (2001), ATN-224 (2006) at ClinicalTrials.gov.
12. Chidambaram MV, Barnes G, Frieden E. J Inorg Biochem. 1984; 22:231. [PubMed: 6097647]
13. Bissig KD, Voegelin TC, Solioz M. FEBS Lett. 2001; 507:367. [PubMed: 11696373]
14. Mandinov L, et al. Proc Natl Acad Sci USA. 2003; 100:6700. [PubMed: 12754378]
15. Pan Q, et al. Cancer Res. 2002; 62:4854. [PubMed: 12208730]
16. Quagraine EK, Reid RS. J Inorg Biochem. 2001; 85:53. [PubMed: 11377695]
17. Suzuki KT, Ogra Y. Res Commun Mol Pathol Pharmacol. 1995; 88:187. [PubMed: 7670850]
18. Juarez JC, et al. Proc Natl Acad Sci USA. 2008; 105:7147. [PubMed: 18480265]
19. Finney LA, O'Halloran TV. Science. 2003; 300:931. [PubMed: 12738850]
20. Pufahl RA, et al. Science. 1997; 278:853. [PubMed: 9346482]
21. Huffman DL, O'Halloran TV. J Biol Chem. 2000; 275:18611. [PubMed: 10764731]
22. Howard JB, Rees DC. Proc Natl Acad Sci USA. 2006; 103:17088. [PubMed: 17088547]
23. Material and methods are available as supporting material on *Science* Online.
24. Rosenzweig AC, et al. Structure. 1999; 7:605. [PubMed: 10404590]
25. Wernimont AK, Huffman DL, Lamb AL, O'Halloran TV, Rosenzweig AC. Nat Struct Biol. 2000; 7:766. [PubMed: 10966647]
26. Zhang C, et al. Eur J Inorg Chem. 2002; 2002:55.
27. Jiguo L, Xinquan X, Zhongyuan Z, Kaibei Y. J Chem Soc Chem Commun. 1991; 1991:249.
28. Dobbek H, Gremer L, Kiefersauer R, Huber R, Meyer O. Proc Natl Acad Sci USA. 2002; 99:15971. [PubMed: 12475995]
29. Zhang L, et al. Biochemistry. 2009; 48:891. [PubMed: 19146437]
30. Itoh S, et al. J Biol Chem. 2008; 283:9157. [PubMed: 18245776]
31. Marston HR. Physiol Rev. 1952; 32:66. [PubMed: 14900035]
32. Mills CF. Philos Trans R Soc London B Biol Sci. 1979; 288:51. [PubMed: 43538]

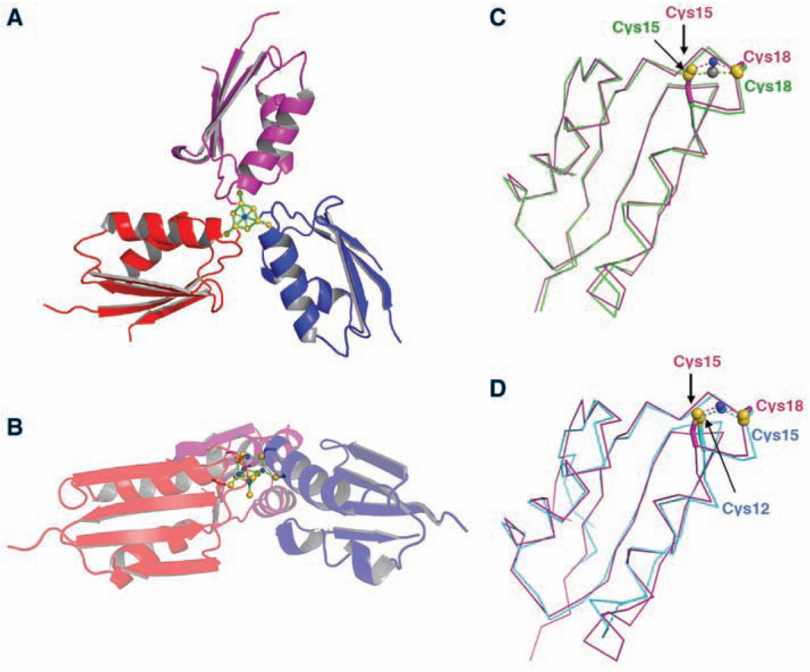

Fig. 1.

Structure of the [TM][(Cu)(Cu-Atx1)$_3$] drug-protein adduct and comparison of Hg-Atx1 and Cu-Atox1 with Cu-Atx1 (monomer B) from the [TM][(Cu) (Cu-Atx1)$_3$] complex (see movie S1). (**A**) Top view of the trimer cluster. (**B**) Side view of the trimer cluster. Atx1 monomers are shown as blue, purple, and red cartoon ribbon diagrams, and copper atoms are shown as blue spheres. The TM- and metal-binding cysteines are represented with a ball-and-stick model, where a molybdenum atom is shown as a cyan sphere, and sulfur atoms are shown as yellow spheres. The coordination bonds are denoted with green dashed lines. Superposition of Cu-Atx1 (monomer B) (purple chain) from the TM-Cu-Atx1 complex with (**C**) Hg-Atx1 (green chain, PDB code 1CC8), and (**D**) with Cu-Atox1 (cyan chain, PDB code 1FEE). Sulfur atoms from Cys^{15} (Atx1) and Cys^{18} (Atx1) are shown as yellow spheres, copper atoms from Cu-Atx1 (monomer B) are shown as blue spheres, mercury atom from Hg-Atx1 is shown as a gray sphere, and copper atom from Cu-Atox1 is shown as a light blue sphere. (Note: TM is not shown.) The similarities of the peptide fold around the metal–binding loop regions in these three structures suggest that binding of Cu by Atx1 in the TM-Cu-Atx1 complex is not disturbed by TM. The Cu coordination environment in Cu-Atx1 from TM-Cu-Atx1 is very similar to the one found in Cu-Atox1 (dimer) (25), but differs with the nearly linear coordination of Hg in Hg-Atx1 (24).

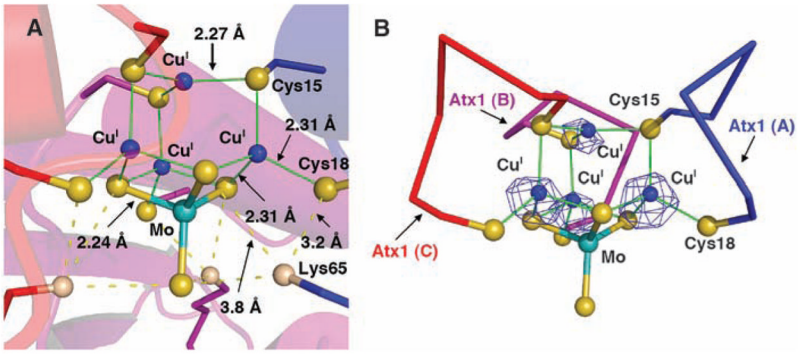

Fig. 2.

Structure of the nest-shaped [$S_6Cu_4MoS_4$] cluster in the [TM][(Cu)(Cu-Atx1)$_3$] trimer complex (see movie S1). (**A**) Structure of the [$S_6Cu_4MoS_4$] cluster with average interatomic distances. The cluster is represented with a ball-and-stick model. Atx1 monomers are as in Fig. 1. Copper atoms are shown as blue spheres; sulfur atoms from Cys^{15} (Atx1), Cys^{18} (Atx1), and TM are shown as yellow spheres; a molybdenum atom is shown as a cyan sphere; and nitrogen atoms from Lys^{65} (Atx1) are shown as tan spheres. The hydrogen bonds are denoted with yellow dashed lines. (**B**) Cu anomalous peaks in the final model of the [$S_6Cu_4MoS_4$] cluster (blue mesh of the anomalous difference Fourier map are contoured at 10.0 σ level). Sulfur atoms from Cys^{15} and Cys^{18} of each of the three Atx1 are connected by blue, purple, and red lines. The molybdenum atom is tetrahedrally coordinated by four sulfur atoms. The top copper atom displays a trigonal-planar geometry and is coordinated by thiolates from Cys^{15} (Atx1), whereas each of the other three neighboring copper atoms adopts a distorted tetrahedral coordination with ligands from both TM and Atx1.

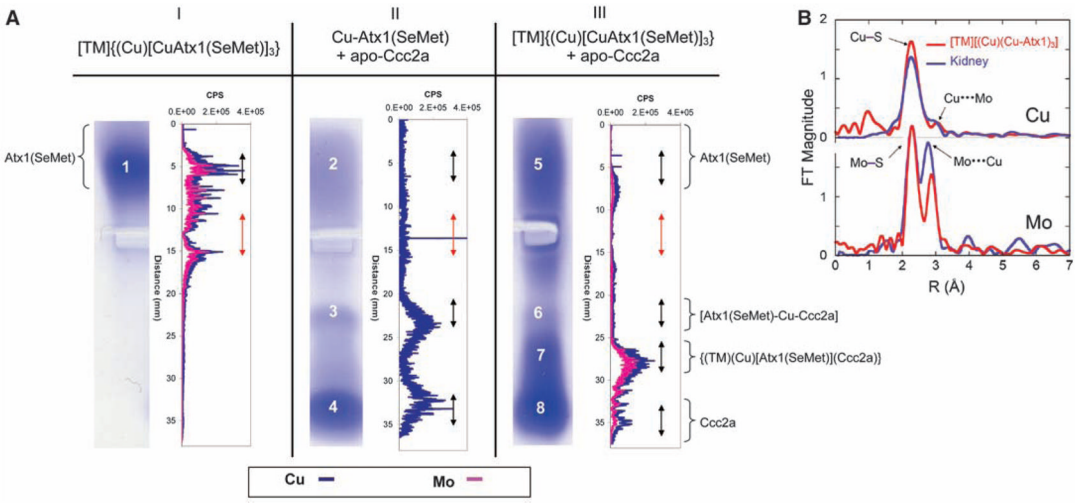

Fig. 3.

TM inhibition of Atx1 copper chaperone activity, and physiological relevance of the [TM][(Cu)(Cu-Atx1)$_3$] complex. (**A**) TM interferes with copper transfer from the Atx1(SeMet) copper chaperone to its target Ccc2a. Inhibition of the copper transfer function was assayed by native gel electrophoresis and qualitative LA-ICP-MS. Gel lanes (I, II, and III) were cut from gel (fig. S6). The [TM]{(Cu)[Cu-Atx1(SeMet)]$_3$} (lane I) is represented by band 1, the Cu-Atx1(SeMet) + *apo*-Ccc2a (1:1) mixture (lane II) yields bands 2, 3, and 4, and the [TM]{(Cu)[Cu-Atx1(SeMet)]$_3$} + *apo*-Ccc2a (1:1) mixture (lane III) yields bands 5, 6, 7, and 8. LA-ICP-MS scans are represented by the intensities (CPS, counts per second) of ^{65}Cu (blue) and ^{95}Mo (pink) (*x* axis), and the length of the gel (mm) (*y* axis). The protein band lengths are shown as black double-headed arrows (↔); the protein loading wells are shown as red double-headed arrows. Excision and gel digestion ICP-MS analysis of band 1 shows a Cu/Mo ratio of 3.6 ± 0.09 (table S1), whereas LA-ICP-MS scans reveal a significant concentration of both metals, leading us to assign band 1 as [TM]{(Cu)[Cu-Atx1(SeMet)]$_3$}. Bands 3 (lane II) and 6 (lane III) are identified as the [Atx1(SeMet)-Cu-Ccc2a] heterodimer complex on the basis of metal and protein analysis of each band. Band 7 contains a mixture of apo-Atx1(SeMet) and apo-Ccc2a with an approximate Cu/Mo ratio of 3.1 ± 0.08 (ICP-MS) (table S1), which is confirmed by a qualitative LA-ICP-MS identification of both metals, indicating the formation of a {(TM)(Cu)[Atx1(SeMet)](Ccc2a)} complex. Elemental analysis by ICP-MS of band 8 reveals copper is at or below the detection limit, indicating that less than 10% of Cu in the TM-Cu-Atx1 complex is transferred to Ccc2a (table S1). Quantitative analysis of the gel slice is consistent with LA-ICP-MS scans showing that most of the Cu of lane III is contained in band 7. These experiments indicate that the formation of the [TM]{(Cu)[Cu-Atx1(SeMet)]$_3$} complex disrupts copper translocation from Cu-Atx1(SeMet) to the domain A of the P-type ATPase Ccc2. (**B**) Cu and Mo K-edge extended x-ray absorption fine structure (EXAFS) Fourier transforms phase-shift overlay (experimental data) for [TM][(Cu)(Cu-Atx1)$_3$], and a kidney sample extracted from LPP rats treated with TM [from (29)]. The slightly higher amplitude of the Mo•••Cu peak for the kidney sample compared with the [TM][(Cu)(Cu-Atx1) $_3$] reflects the slight difference in the Mo EXAFS best fits, 3 and 2–3 Mo•••Cu, respectively. The Cu•••Mo peak is slightly more intense for the [TM][(Cu)(Cu-Atx1)$_3$] complex than for the kidney sample, modeled by 1 Cu•••Mo instead of 0.5, respectively. Cu and Mo K-edge EXAFS spectra and EXAFS Fourier transform including experimental data and best fits are included in figure S13. The fit results are summarized in table S2.